



Article

Upgraded Low-Frequency 3D Lightning Mapping System in North China and Observations on Lightning Initiation Processes

Mingyuan Liu ^{1,2}, Xiushu Qie ^{1,2,*}, Zhuling Sun ¹, Rubin Jiang ¹, Hongbo Zhang ¹, Ruiling Chen ^{1,2}, Shanfeng Yuan ¹, Yu Wang ^{3,4} and Xiangke Liu ⁵

- ¹ Key Laboratory of Middle Atmosphere and Global Environment Observation, Institute of Atmospheric Physics, Chinese Academy of Sciences, Beijing 100029, China; lium@mail.iap.ac.cn (M.L.); sunzhuling@mail.iap.ac.cn (Z.S.); zhanghb@mail.iap.ac.cn (H.Z.); yuanshanfeng@mail.iap.ac.cn (S.Y.)
- ² College of Earth and Planetary Sciences, University of Chinese Academy of Sciences, Beijing 100049, China
- ³ State Grid Electric Power Research Institute Wuhan NARI Limited Liability Company, Wuhan 430206, China
- ⁴ State Grid Electric Power Research Institute Co., Ltd., Nanjing 211199, China
- ⁵ Key Laboratory for Meteorological Disaster Prevention and Mitigation of Shandong Province, Jinan 250031, China
- * Correspondence: qiex@mail.iap.ac.cn

Abstract: The three-dimensional (3D) low-frequency lightning mapping system (LF-LMS) in north China has been updated. The lightning electric field derivative (dE/dt) sensor and continuous acquisition mode has been newly designed to ensure a capability of entire lightning processes detection, especially weak discharges during lightning the initiation process. The twice cross-correlation delay estimation and the grid iteration nested optimization location algorithm are used to realize the 3D location of the discharge channel, and the location resolution and calculation speed are balanced consequently. The location results of the rocket-triggered lightning demonstrated that the system achieved a high-resolution mapping of lightning discharge channels, which coincided well with the optical images. The horizontal and vertical location error for rocket triggered lightning was less than 40 m in both horizontal and vertical. Intracloud (IC) lightning flashes were observed to be initiated by three different discharge processes, initial breakdown pulse (IBP), narrow bipolar event (NBE), and initial E-change (IEC). The corresponding initial height was 10.5 km, 6.9 km, and 9.2 km, respectively. The upward negative leader was initially located, followed by scatter radiation sources and negative recoil leaders in the lower negative charge region for all cases. The electric field characteristics of the IEC and subsequent IBPs indicated that they are different discharge processes with the same current direction. The IEC process might correspond to the discharge process with continuous current and less noticeable current changes.

Keywords: 3D lightning mapping system; lightning initiation; low-frequency; dE/dt sensor



Citation: Liu, M.; Qie, X.; Sun, Z.; Jiang, R.; Zhang, H.; Chen, R.; Yuan, S.; Wang, Y.; Liu, X. Upgraded Low-Frequency 3D Lightning Mapping System in North China and Observations on Lightning Initiation Processes. *Remote Sens.* **2024**, *16*, 1608. <https://doi.org/10.3390/rs16091608>

Academic Editor: Yuriy Kuleshov

Received: 10 April 2024

Revised: 28 April 2024

Accepted: 29 April 2024

Published: 30 April 2024



Copyright: © 2024 by the authors. Licensee MDPI, Basel, Switzerland. This article is an open access article distributed under the terms and conditions of the Creative Commons Attribution (CC BY) license (<https://creativecommons.org/licenses/by/4.0/>).

1. Introduction

It is generally believed that lightning electromagnetic waves with different wavelengths can reflect different discharge processes in various space scales, which lays the basis of lightning detection technology and the study on lightning discharge process. The very high-frequency (VHF) bands are usually used to determine the precise location of lightning channels, such as breakdown processes, stepped leaders, and recoil leader discharges, while low-frequency (LF) or very low-frequency (VLF) bands are typically only used to detect the large-scale discharge processes, such as return strokes, leaders, or intense discharges within clouds [1].

Recently, the LF and VLF bands have been widely used for three dimensional (3D) lightning channel mapping [2–10]. The principle of LF/VLF 3D lightning location algorithms is time-of-arrival (TOA), which promisingly locates the spatiotemporal evolution of

the lightning radiation source by utilizing the differences in the arrival times of electromagnetic radiation signals from the same lightning radiation source at distributed lightning detection stations. In recent years, significant advancements have been made in the field of three-dimensional (3D) lightning location technology using VLF/LF bands, enabling high temporal resolution location of lightning channels, as explained in the following.

The TOA lightning location process involves extracting waveform or peak information from the time series of radiation signals from a same lightning source observed at various distributed detection stations. Furthermore, a reliable and efficient optimization method is necessary to compute the spatiotemporal location of the radiation source. This LF/VLF-based lightning location technique has deepened our understanding of lightning development and evolution. Karunarathne et al. [11] established the PBFA (position by fast antenna) system consisting of 10 stations operating in the frequency range of 1.6–630 kHz, and found that in the early stage of lightning, pulse location results in the LF/VLF frequency range were better than those in the VHF range. Wu et al. [4] established the FALMA (fast antenna lightning mapping array) system comprising 12 stations, detecting an effective frequency range from 500 Hz to 500 kHz, with a sampling rate up to 25 MS/s and sampling length of 1 s, and presented a good performance in mapping lightning return strokes, stepped leaders, K-processes, and lightning initial pulses. Wang et al. [3] introduced a 16-station BLNET (Beijing Lightning NETWORK), which operated in the frequency range of 1.5 kHz to 2 MHz, enabling real-time 3D location of lightning and tracking of thunderstorm development.

A significant development was the application of interferometry algorithms. Lyu et al. [2], introduced the cross-correlation method in the lightning interferometry to calculate signal delays in the long-baseline LF lightning location system, and then utilized the TOA optimization algorithm to determine the 3D channel development of lightning. Stock et al. [6] developed two methods for mapping lightning in the LF band, one was a hybrid TOA-interferometric algorithm similar to Lyu [5], and the other was a purely interferometric algorithm, which produced images of the 3D coherence of the LF lightning signals. Then, Zhu et al. [7] elaborated on the purely interferometric algorithm, which involves calculating the 3D total correlation of lightning signals received by different stations and locating lightning with the maximum correlation in space, as different from the traditional TOA method. These methods help to obtain information about weak or visually indistinguishable discharges, allowing LF networks to locate more lightning sources even with resolutions comparable to those of VHF-based systems, compared to using only the peak of the lightning signal at each site.

These networks and algorithms provide precise source locations and insights into the dynamics of lightning discharge channels [9,12]. Compared to the VHF band, lightning location networks in the VLF band yield less data, suitable for continuous lightning monitoring of the entire thunderstorm process. This allows for depicting the evolution of the entire lightning event's radiation source over time, including the lightning initiation processes.

Since the lightning initiation mostly occurs within clouds and is difficult to observe directly, a primary method to reveal its characteristics is to detect the electromagnetic radiation signals and determine the spatiotemporal location of the radiation source with high resolution. The lightning initiation is commonly believed to involve the initial breakdown pulses (IBPs), which typically manifest as a series of pulses with different amplitudes, polarities, and widths on the electric field change waveform [13–15].

Recently, Marshall et al. [16,17] discovered the presence of an initial E-change (IEC) with a duration of 0.1–6 ms preceding the first traditional IBP. This IEC is accompanied by VHF radiation discharge and is considered to be an ionization event that enhances the local electric field, leading to the generation of the first initial pulse. The narrow bipolar event (NBE) has also been observed as the lightning initiation process and followed by the IBPs [18,19]. The mechanisms behind the generation of the initial breakdown pulse and different types of lightning initiations remain unclear. In order to investigate the initial

discharge process of lightning, it is crucial to have high-sensitivity continuous detection and high spatiotemporal resolution radiation source localization.

Since the summer of 2005, continuous experiments involving rocket-triggered lightning and severe convective weather observations have been conducted in Binzhou City, Shandong Province, situated in North China [20,21]. With the aim of achieving high-resolution 3D locations of lightning discharge channels, a LF 3D Lightning Location system (LF-LMS) around the rocket-triggered experiment base has been established since 2016 [17]. Continuous improvements are being made to the detection hardware and the location algorithm. In this paper, we present the newly developed lightning electric field derivative (dE/dt) sensor and location algorithm, along with the 3D location of one rocket-triggered lightning flash. Furthermore, three types of lightning initiation for intracloud (IC) flashes in the same thunderstorm are analyzed in detail based on the 3D mapping results on the lightning processes.

2. Instrumentation

Figure 1 shows the layout of the 3D LF-LMS around the rocket-triggered lightning experiment base. The LF-LMS comprised 8 time-synchronized detection stations, with the baseline lengths ranging from about 6 to 38 km between each other. The lightning detection sensor, time synchronization device, and acquisition system for the upgraded LF-LMS will be introduced in this section.

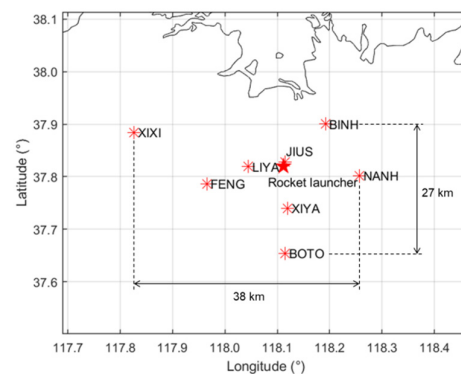


Figure 1. Layout of the 3D LF-LMS of eight stations (red asterisk) in 2022. The red star marks the rocket launcher (position of lightning rod) in the Triggering Lightning Experiment (SHATLE).

2.1. Lightning Electric Field Derivative (dE/dt) Sensor

The dE/dt sensor was designed for efficient lightning detection with high gain. Figure 2 shows the schematic of the dE/dt sensor's front-end circuit. This sensor was equipped with a metal plate as an antenna, and the I/V converter was employed for amplification and current transfer to voltage output.

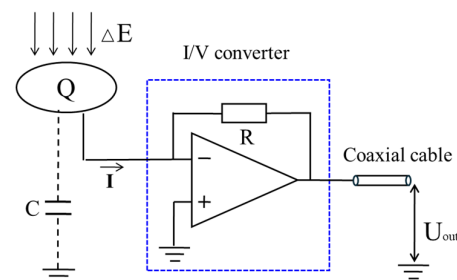


Figure 2. Simplified schematic of the lightning electric field derivative (dE/dt) sensor front-end circuit.

The change of the electric field induces a charge on the plate, resulting in the transfer of an equal amount of opposite charge, thereby forming a current denoted as I . In the I/V converter, there is a feedback mechanism that the operational amplifier ensures

equalization of voltages at its two input terminals. This is achieved by grounding the non-inverting (positive) input, causing the inverting (negative) input to act as a “virtual ground”. Therefore, the electrical potential of the plate, connected to the inverting input, is equivalent to that of the ground, even if it is not directly connected to the ground. This output voltage is inversely proportional to the electric field derivative radiated by lightning, as shown in the following formula:

$$U_{\text{out}} = -IR = -\varepsilon_0 AR \times \frac{dE}{dt} \quad (1)$$

where A represents the effective sensing area of the antenna, it is usually larger than the actual area of the plate due to the elevated installation of the antenna, which enhances local electric field distortions. This factor depends on the surrounding environment and height above ground. Additionally, ε_0 represents the dielectric constant of air, and R stands for the resistance value in the feedback loop. Adjusting this resistor value can adjust the sensor sensitivity. This dE/dt sensor can achieve faster response times and avoid the distortions that may be introduced by these electrical distributed parameters. It was confirmed that this sensor is suitable for measuring small current signals.

Figure 3 shows the waveform comparison on the dE/dt and the fast electric field change (E-Change) synchronously detected by the dE/dt sensor and a fast antenna. Because the dE/dt sensor operates without a time constant, the dE/dt waveform can recover within a few microseconds after encountering a large signal, without compromising the detection of subsequent pulses. Thus, the dE/dt sensor can provide higher gain and more sensitive pulse detection. Meanwhile, the fast electric field change signal is used to better distinguish the types of lightning discharges. In the LF-LMS, the bandwidth of the dE/dt sensor and the fast antenna is 100 kHz to 800 kHz and 1.5 kHz to 1 MHz, respectively.

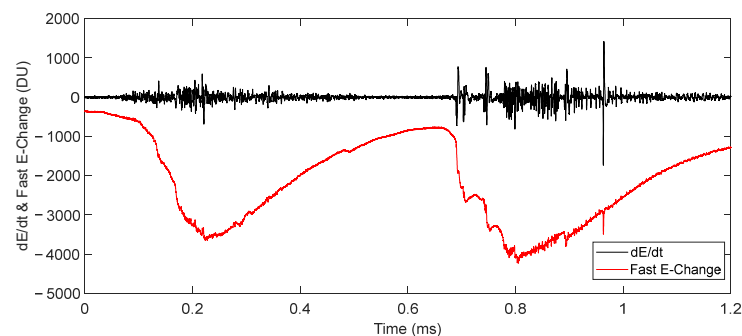


Figure 3. Comparison of dE/dt waveform (black) detected by dE/dt sensor and the fast E-change waveform (red) detected by the fast antenna with a time constant of 0.1 ms, synchronized for detection.

2.2. Hardware Component of the Distributed Stations

Each station was equipped with a dE/dt sensor, a GPS disciplined oscillator (GPSDO) synchronized clock, and high-speed data acquisition and recording devices.

The GPSDO synchronized clock was employed, integrating the short-term stability of an internal oven-controlled crystal oscillator (OCXO) with the long-term accuracy derived from satellite atomic clocks. This clock provided a reliable time reference for each substation, ensuring precise measurement of the time difference in lightning signal propagation to each station. The acquisition system used the GPSDO synchronized clock signal as the reference, securing the accuracy of the sampling clock. The 1PPS (pulse per second) signal, which served as the time synchronization signal for distributed stations, was stabilized by the GPSDO clock before output. This stabilization effectively reduces jitter in the original GPS 1PPS signal caused by atmospheric conditions. Laboratory tests show that the time discrepancy between 1PPS signals from two independently operating GPSDOs is less than 20 ns. By utilizing NMEA0183 time information from the GPS, along with the stabilized 1PPS signal and the high-precision sampling clock, the system can determine the absolute

time (standardized to Coordinated Universal Time, UTC) corresponding to each acquired sample, with a resolution identical to the system's sampling period.

Previously, the LF-LMS adopted the ABA mode for the lightning data acquisition [17], involving segments of low-speed continuous collection (A) and high-speed triggered collection (B). Specifically, during segment A, data were continuously collected at a low sampling rate of 400 kS/s; for segment B, upon meeting the trigger condition, data were collected at a high sampling rate of 10 MS/s for a duration of 840 milliseconds. To achieve comprehensive observation of passing thunderstorms, the current approach was upgraded to a continuous nonstop data recording mode at a sampling rate of 20 MS/s with a 16-bit vertical signal resolution. It employed the DMA (direct memory access) and ring buffer technology, to enable uninterrupted recording throughout the thunderstorm.

As mentioned earlier, the detection of relatively high-frequency pulse signals by the dE/dt sensor presents waveforms fluctuating around zero during the lightning process, without significant low-frequency trend changes. This makes it more accurate when searching for waveform peaks and matching pulses but makes it difficult to distinguish various lightning types and discharge subprocesses from the dE/dt pulse signals. Therefore, a fast antenna with a time constant of 0.1 ms was equipped in the LIYA central station of the LF-LMS to identify the physical processes of lightning discharge, as shown in Figure 3. In the following analyses, the definition of lightning electric field polarity follows the physics convention, where the electric field direction vertically upwards is considered positive.

3. Lightning Radiation Source Location Method

The lightning 3D location process includes signal preprocessing, waveform matching, and location calculation. Initially, signal quality is enhanced through filtering with the empirical mode decomposition (EMD) method. Twice cross-correlations were then employed to determine the time differences of signal arrival.

Subsequently, the Chan optimization algorithm [3,22] was adopted to establish the initial location result of the radiation source. The initial value was then refined and optimized by the 3D mesh nested iterative search algorithm, which is helpful for the high spatial resolution 3D location results of lightning radiation signals. Each step is explained in the following sections.

3.1. Signal Preprocessing

The signals received from each station underwent signal processing firstly, aimed at effectively suppressing noise and accentuating signal characteristics to enhance data quality.

Typically, lightning location networks operating in the LF band have detection frequencies not exceeding 500 kHz [5,8]. The LF-LMS, aiming to leverage the broadband characteristics of the dE/dt sensor, employed the EMD method for signal preprocessing and opted not to use the bandpass filtering common in other lightning location networks.

The EMD method simplifies the analysis of complex, variable signals by breaking them down into intrinsic mode functions (IMFs) [6], revealing underlying patterns and trends. The EMD method was employed to effectively eliminate waveform offsets, trends, and specific interference frequencies. The methodology includes several steps:

1. Background noise analysis: A segment of waveform data without lightning signals is selected for Fourier spectral analysis to identify noise signal frequencies. The whole waveform data are then divided into fixed-time windows for subsequent lightning signal extraction.
2. EMD process: The data within each time window are decomposed into multiple IMFs using the EMD method. Each IMF undergoes Fourier spectral analysis to determine its peak frequency.
3. Signal reconstruction: IMFs free from background noise and low-frequency trends are combined and reconstructed into new waveforms. Figure 4 shows an original signal and 9 IMFs obtained using the EMD method, with IMF 5–9 exhibiting significant

low-frequency interference. Consequently, IMFs 1–4 are combined and reconstructed to generate the signal without noticeable interfering signals.

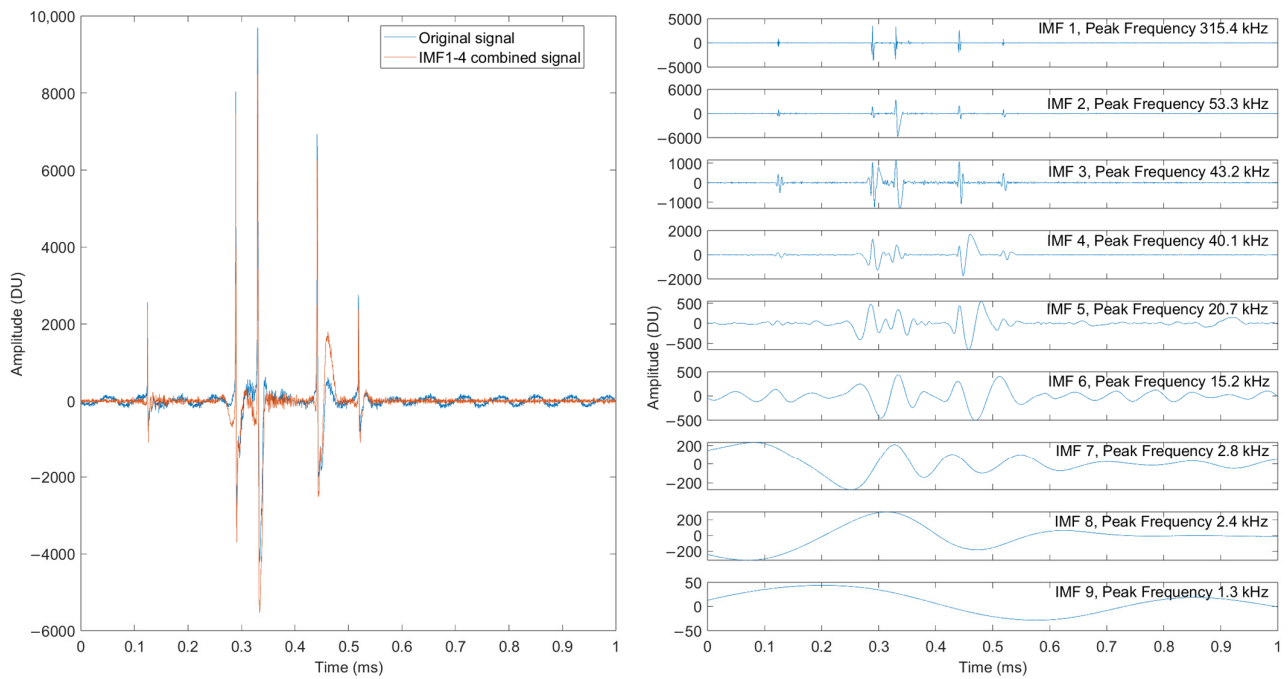


Figure 4. The original signal and signals reconstructed by the accumulated IMF1–4 (left), along with the signals of each IMF obtained from the EMD method (right).

3.2. Waveform Matching

In this process, waveforms from distributed stations are matched with those of the main station to get time differences of arrival.

The propagation of lightning signals changes with distance, displaying different decay rates for its electrostatic field, induction field, and radiation field [23]. Lightning radiation waveforms detected at different stations may exhibit different characteristics and even varying polarities. To solve the problem of low correlation caused by the change of waveform between stations, the Hilbert transform is adopted to calculate the instantaneous amplitude of the signal and compare it between stations. Figure 5 shows the waveform of dE/dt and the waveform of instantaneous amplitude after Hilbert transform processing.

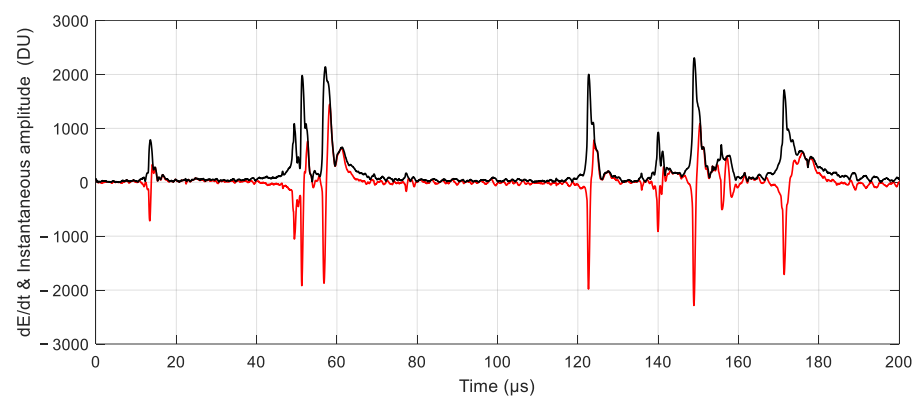


Figure 5. Comparison of dE/dt waveform (red) and instantaneous amplitude waveform after Hilbert Transform (black).

Subsequently, the waveform pulses in the main station (JIUS) are identified. Following the identification of peak time information, a larger 75 μs time window, centered on

the identified peak, is utilized to extract data from the corresponding time intervals at all detection stations. The generalized cross-correlation algorithm is then employed to determine the time delays of signals relative to the main station. Using these time delays, the occurrence time of pulse signals across all stations is roughly aligned.

Data encompassing these preliminarily aligned peaks, extending 12.5 μs on either side, are then extracted and interpolated onto a high-resolution of 1 ns time scale. A more precise time delay within this finer window is achieved through the second generalized cross-correlation. The delay information from both the larger and smaller time windows is combined to determine the time difference of lightning signals.

3.3. Locating Calculation

Upon acquiring the time difference data between the central station and the other stations, the LF-LMS employs a series of optimization algorithms to accurately determine the location of the lightning radiation source.

Firstly, the initial result is computed by the Chan algorithm, which is a classical non-recursive algorithm with analytic expression solutions based on the two-step weighted least square method [3,22]. The LF-LMS detection stations are located almost on a plain, where the height difference between each station is small. This leads to significant errors in height in the Chan algorithm's 3D calculation results. Therefore, only the two dimensions (2D) result of the Chan algorithm is utilized as the initial value for further computations.

The initial 2D result is extended to form a horizontal centroid, constructing a local spatial grid extending vertically from 0 to 15 km. The grid size is 500 m \times 500 m \times 15 km, divided into grid steps of 50 m \times 50 m \times 150 m. Within this space, calculations are performed for each grid point to determine the theoretical signal propagation time differences between these points and the main station and the other stations.

The χ^2 discrepancy formula is as follows:

$$\chi^2 = \sum_{k=1}^{N-1} \frac{(\Delta T_k^{\text{obs}} - \Delta T_k^{\text{thr}})^2}{(N-4)\sigma^2} \quad (2)$$

where k represents the station number, N represents the total number of stations, and $N-4$ equals the degrees of freedom of the Chi-square χ^2 distribution. ΔT_k^{obs} and ΔT_k^{thr} represent the observed and theoretical time differences of signal propagation to the k th station and the main station. σ stands for the average root mean square (RMS) timing error of each site. Its estimation involves fitting the theoretical χ^2 distribution to the observed χ^2 distribution [24,25]. Figure 6 shows the evaluated results, with the assessment outcome for the location system introduced in this paper being about 110 ns. Rooted in the principle of minimizing χ^2 , this guides the selection of the optimal grid point, which then becomes the initial value for the subsequent round of optimization.

Subsequently, through multiple iterations, the optimal grid point can be selected to achieve higher-resolution results. It begins with a spatial grid configuration of 5 \times 5 \times 11 and a spatial step of 16 m.

The process is dynamic, adjusting its grid center points based on results of the previous iteration. As the step size is halved in every subsequent iteration, it leads to increasingly finer resolution. By employing this method, a high resolution of 2 m can be achieved after four iterations. For this time window, the precise 3D location of lightning is determined at the grid point with the minimum χ^2 value. Finally, only the location results within the 95% confidence intervals are considered reliable and retained in the final outcome.

Based on the estimation of timing error, Monte Carlo error analysis was employed to evaluate the location accuracy of the station network. The method creates a grid in the evaluation space and adds random errors to theoretical values based on the time of arrival at each station. These errors follow a zero-mean normal distribution with an RMS error of 110 ns. Using the arrival time calculated with added error, the location result is computed, and compared with the real position to obtain the location error. The difference between

the calculated location result with added time error and theoretical values is compared to evaluate accuracy. The horizontal and vertical location errors (at altitudes above 3 km) are less than 100 m in the center of the network and less than 200 m within all the coverage of the network.

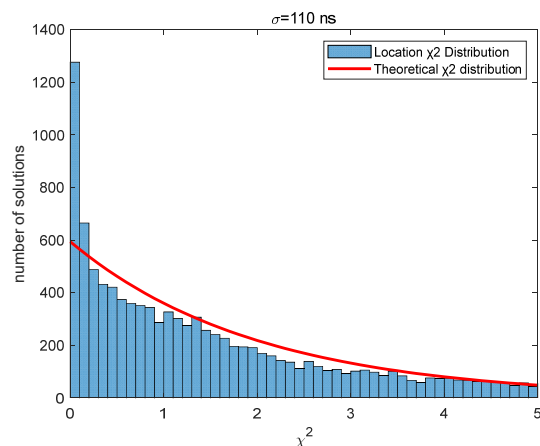


Figure 6. Observed χ^2 distribution (histogram) and theoretical χ^2 distribution (red), where the number of stations is 6, degrees of freedom are 2, and the calculated average RMS timing error σ equals 110 ns.

The upgraded LF-LMS utilizes the initial values provided by the Chan algorithm to dynamically compute a small volume grid as needed, maintaining high resolution while minimizing computational load. A parallel computing technique is employed to enhance calculation speed. This method does not have convergence issues, and the results can be constrained within a specific region, corresponding to the height range of the thunderstorm cloud.

4. Lightning Location Results of a Rocket-Triggered Lightning Flash

In this section, we present detailed mapping results of a rocket-triggered lightning flash. The results effectively demonstrate the advanced capabilities of the 3D lightning location system in detecting and localizing lightning discharge channels. In the lightning cases described hereafter, all location results are referenced to the coordinates of the JIUS station located at the center of the network, serving as the origin point for both horizontal and vertical directions.

On 13 August 2020, during a rocket-triggered lightning experiment, a negative polarity lightning flash was successfully triggered. Synchronized data were collected from a total of six detection stations in the network. The mapping results, as shown in Figure 7, depict the 3D progression of this lightning radiation source and its evolution over time. The duration of this triggered lightning was about 0.5 s and contained two negative return strokes. The LF-LMS effectively captured the upward positive leader at the initial stage, as well as the development and extension of the lightning channel within the cloud.

Figure 8 illustrates the 2D location results of the initial stage of the triggered lightning overlaid with an optical image, with the JIUS station as the coordinate origin. This optical detection was captured using a synchronized high-speed camera. The continuously developing upward leader was initiated from the tip of the wire carried by the rocket; the first radiation pulse should be initiated from the wire tip, as shown by the top of the straight channel. The LF-LMS location result indicated that leader originated about 16 m horizontally and 40 m vertically apart from the wire tip, as shown in Figure 8. Due to this comparison based on a 2D optical image, the 3D error may be slightly larger. The location for this rocket-triggered lightning demonstrated the capability of the 3D lightning location system to precisely map the lightning discharge channels. Furthermore, the LF-LMS in-

tricately depicts discharge channels outside the optical camera field of view and channels within thunderclouds, which are not the focus of this paper.

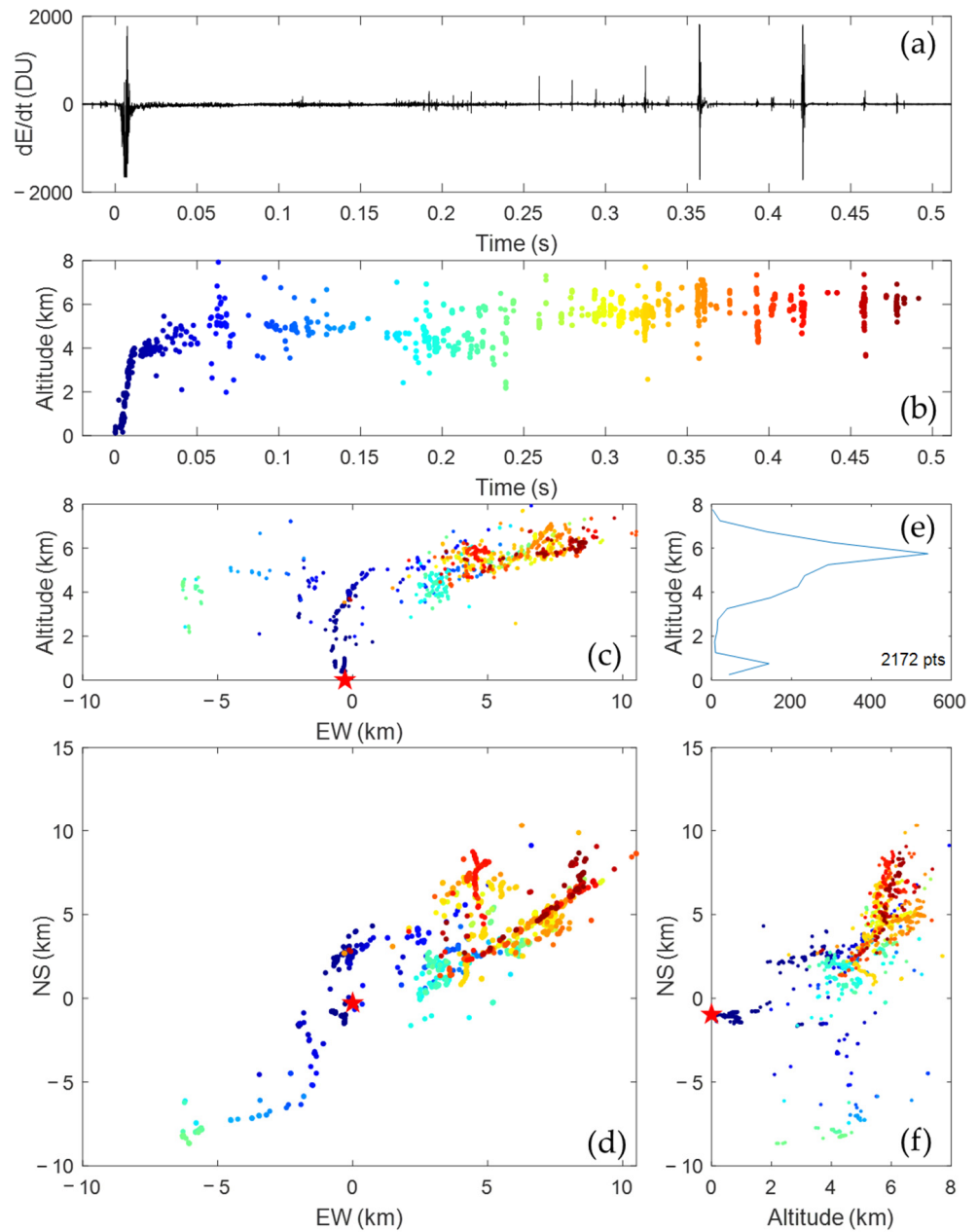


Figure 7. The 3D location results of a negative rocket-triggered flash on 13 August 2020. (a) The waveform of dE/dt . (b) The location result in the height–time view, with color changing from blue to red according to time. (c) Height–distance (from west to east) view. (d) Plan view. (e) Source distribution along the height. (f) Distance (from south to north)–height view. The red star symbolizes the rocket launcher. The coordinate origin corresponds to the position of the JIUS station.

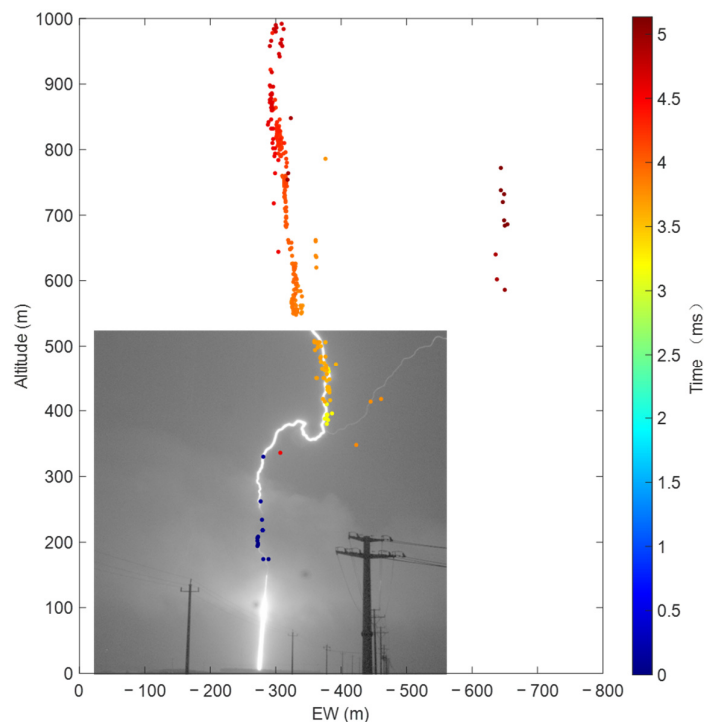


Figure 8. The location results of triggered lightning are displayed in 2D and overlaid with optical detection of the initial-stage frame, captured by a synchronized high-speed camera. The color changes from blue to red starting from the moment of the first location result.

5. Initiation Discharge of IC Lightning Flashes and Their Subsequent Discharges

In this section, we will present three IC lightning flashes that occurred during the same thunderstorm on 13 August 2020. The thunderstorm over the network lasted for over 2 h, with continuous recordings of lightning activity from six stations throughout the thunderstorm event. The three IC lightning flashes occurred within a span of 20 min, each corresponding to three distinct characteristics of lightning initiation.

5.1. Lightning Initiation by the Classic Initial Breakdown Pulse

Figure 9 presents a detailed location result of an IC lightning flash that initiated with a classical initial breakdown pulse at 12:22:54 local time. This IC flash lasted for about 780 ms. Based on analysis of radiation source density, the speed of channel development, electric field waveform changes, and the observed recoil leader process, the polarity characteristics of the leader discharge could be determined.

During initiation stage of the IC flash, the network firstly captured the development of an upper negative leader channel and expanded horizontally at the upper region of the lightning initiation area. About 210 ms after the lightning initiation, the leader channel changed its direction to descend diagonally, reaching a minimum height of 6 km and spanning 36 km from the initiation area. The average speed of this channel development process was 1.1×10^5 m/s, indicating that the channel developed within a positive charge region of the cloud.

About 20 ms after the lightning initiation, a positive leader channel was detected, which initially descended vertically from its origin with a vertical channel length of 1.5 km. After reaching an altitude of 8.5 km, it branched into two channels, and continued to develop at an average velocity of 1.1×10^4 m/s in a negatively charged region at 5–8 km. Multiple negative recoil leader processes were detected moving toward the lightning initiation area in the same region. Based on the mapping results, it can be revealed that the IC flash was of the positive IC type, occurring within a dipolar charge structure with an upper positive charge region and a lower negative charge region.

Figure 10 shows the location results of this lightning event during the initial 60 ms. The lightning started at an altitude of 10.4 km and produced the first initial breakdown pulse (IBP). The negative leader initially inclined upwards for 5 ms and then transitioned to a horizontal trajectory, forming a vertical channel approximately 300 m long. The 3D speed of this negative leader was 6×10^4 m/s. At 54 ms following the lightning's start, scattered sources associated with the positive leader were detected descending from the initiation area.

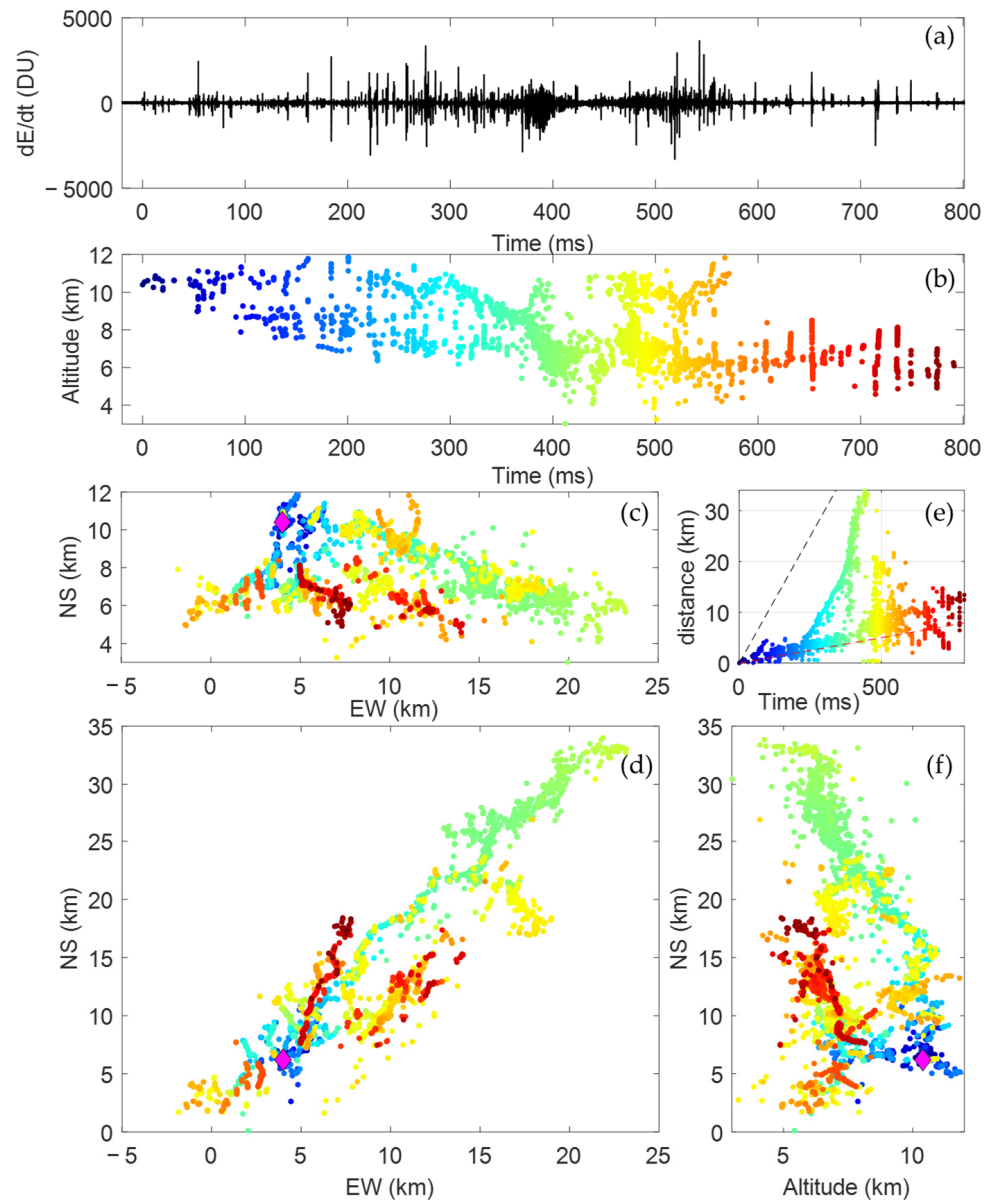


Figure 9. The entire location result of the IC lightning initiated by an initial breakdown pulse. (a) The waveform of dE/dt . (b) The location result in the height–time view, with color changing from blue to red according to time. (c) Height–distance (from west to east) view. (d) Plan view. (e) Change in distance of radiation sources from initiation point over time. The red dashed line indicates a reference speed of 10^4 m/s, black dashed line represents a speed of 10^5 m/s. (f) Distance (from south to north)–height view. The magenta diamond stands for the initial point.

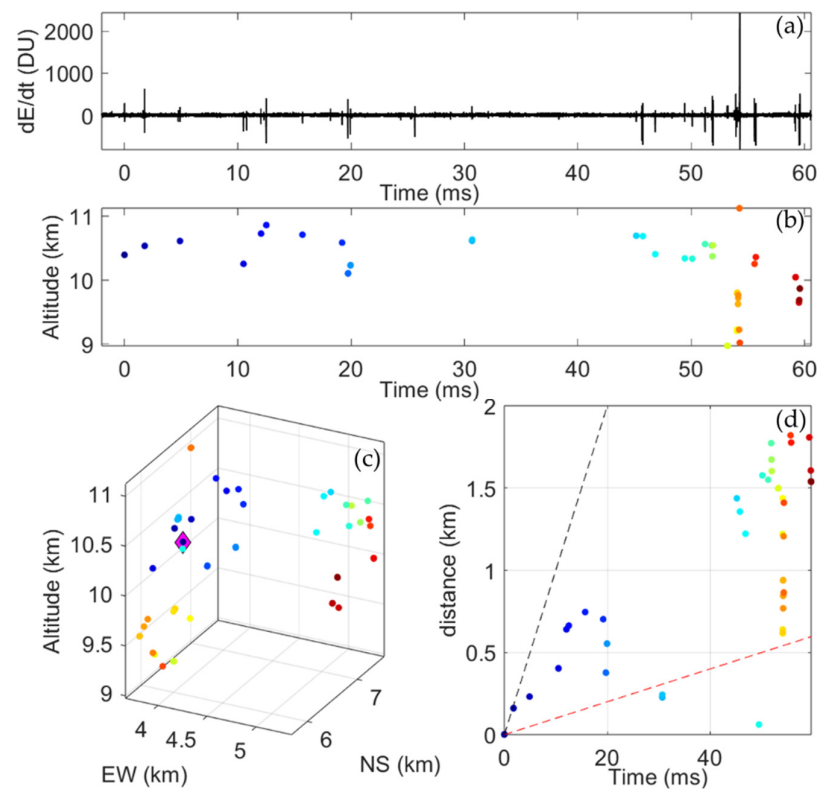


Figure 10. The location result of the IC lightning during the initial 60 ms. (a) dE/dt waveform, (b) location result in height–time view, with color changing from blue to red according to time. (c) 3D view. The magenta diamond stands for the initial point. (d) Change in distance of radiation sources from initiation point over time. The red dashed line indicates a reference speed of 10^4 m/s, and the black dashed line represents a speed of 10^5 m/s.

5.2. Lightning Initiation by the Bipolar Narrow Pulse

Figure 11 shows the waveform data and 3D location results of a narrow bipolar event (NBE)-initiated IC lightning, that occurred at 12:02:39 local time. The lightning flash lasted 665 ms. The results indicated that the lightning flash originated at ~ 7 km altitude with a narrow bipolar pulse in the electric field change waveform and exhibited a two-layer structure overall. The upper negative leaders primarily developed within the positive charge region, while the lower positive leaders mainly developed within the negative charge region. The IC lightning flash was also of the positive IC type.

About 0.4 ms after the lightning initiation, a typical IBP with the same polarity as the NBE pulse was detected, corresponding to the negative leader ascending from the lightning initiation point. Subsequently, the lightning leader branched into two channels, at an altitude of 8.2 km. One channel terminated at 140 ms after the lightning initiation, with development within a height range of 6.2 to 8.8 km, and the farthest tip was located 5 km away from the lightning initiation area. Another channel stopped extending outward approximately 255 ms after initiation, with the channel covering a height range of 5 to 9.5 km and reached a distance of 22.5 km away.

About 245 ms after the lightning initiation, scattered discharges occurred below the initiation area. Subsequently, at 576 ms, a negative recoil leader was detected along the existing positive channel, passing through the lightning initiation area and developing far away from the initiation area along the original negative channel. The positive leader channel primarily developed within a height range of about 3 to 6 km below the lightning initiation area, corresponding to a negatively charged region involved in the discharge.

The mapping results of this IC flash revealed the involvement of positive and negative charge regions during the discharge process, indicating a two-layer distribution. Both

upper and lower layers exhibited similar horizontal positions, but they differed in their extent. This distribution might be attributed to variations in charge distribution within the thundercloud.

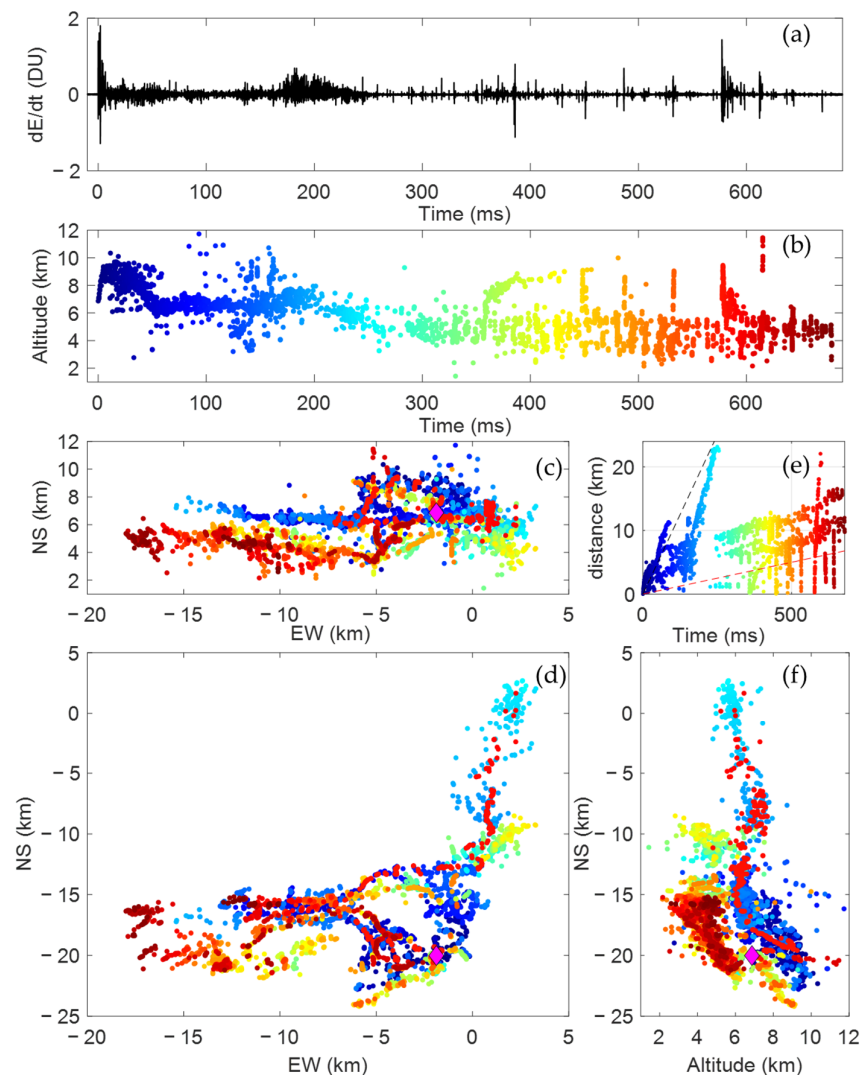


Figure 11. The entire location result of the IC lightning initiated by an initial breakdown pulse. (a) The waveform of dE/dt , (b) The location result in the height–time view, with color changing from blue to red according to time. (c) Height–distance (from west to east) view. (d) Plan view. (e) Change in distance of radiation sources from initiation point over time. The red dashed line indicates a reference speed of 10^4 m/s, and the black dashed line represents a speed of 10^5 m/s. (f) Distance (from south to north)–height view. The magenta diamond stands for the initial point.

Figure 12 shows the 3D lightning location results and electric field waveform during the initial stage of this lightning event. The NBE pulse with a width of $15 \mu\text{s}$, was located at a height of 6.9 km. During the first half-cycle of the NBE pulse, the waveform exhibited fast positive changes. The VHF interferometer imaging results [26] (which are not presented here) showed that the associated VHF discharge sources initially descended, accompanied by positive changes in the electric field, indicating that this NBE event corresponded to the fast positive breakdown developing downward. About 0.4 ms after the NBE, clusters of initial breakdown pulses appeared. These pulses corresponded to leaders developing upward from the lightning initiation area at a 3D velocity of 6.7×10^5 m/s.

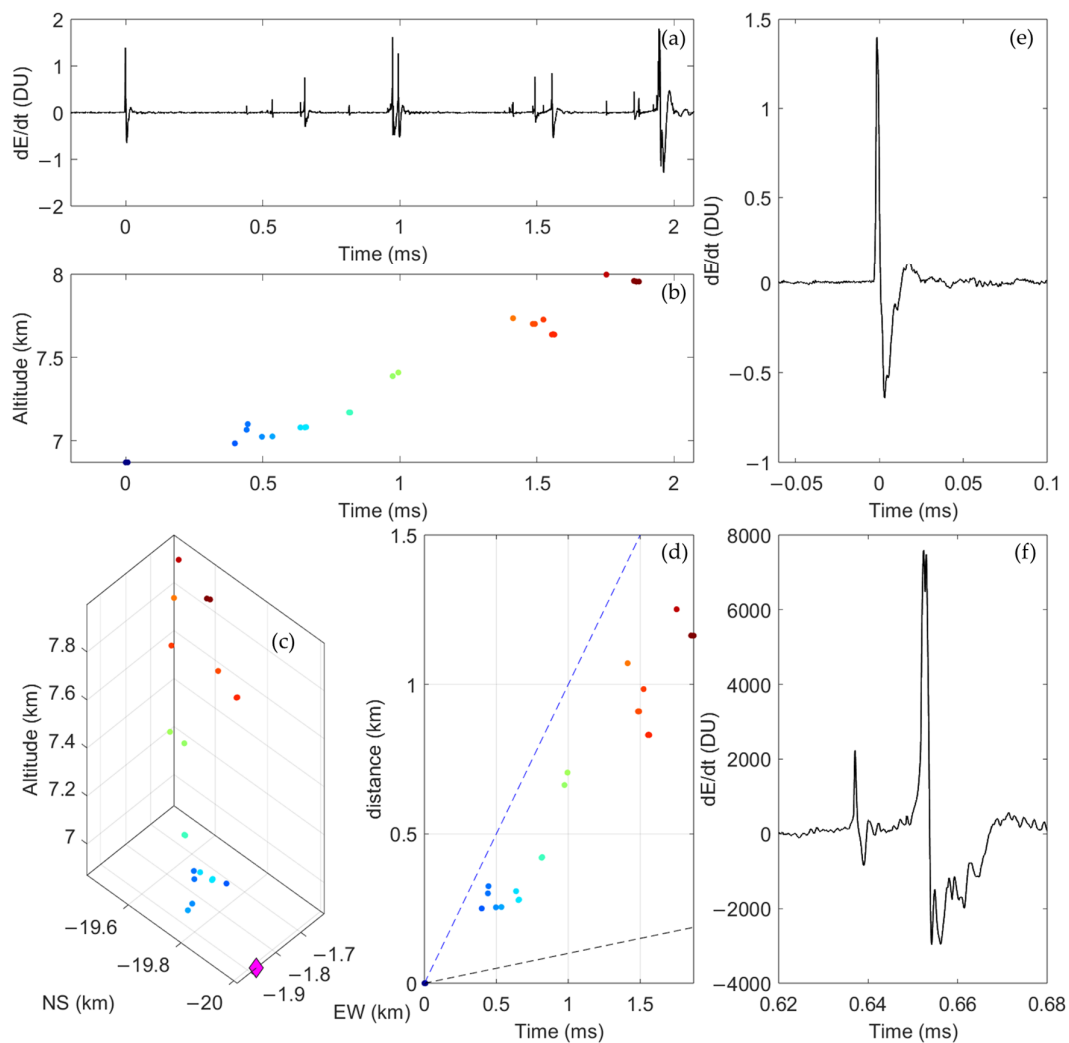


Figure 12. The location result of the NBE-initiated IC lightning during the initial 2 ms. (a) dE/dt waveform, (b) location result in height–time view, with color changing from blue to red according to time. (c) 3D view. The magenta diamond stands for the initial point. (d) Change in distance of radiation sources from initiation point over time. The blue dashed line indicates a reference speed of 10^6 m/s, and the black dashed line represents a speed of 10^5 m/s. (e) The dE/dt waveform of NBE. (f) The dE/dt waveform of the breakdown pulse following the NBE.

5.3. Lightning Initiation by Initial E-Change (IEC)

Before the classical initial breakdown phase in an IC lightning flash occurred on 13 August 2020, at 12:15:42, a preliminary, initial E-change (IEC) was detected, and the waveform of the IEC was evident in the fast antenna waveforms synchronized with the lightning location system.

The waveform along with the location result for this entire IC discharge process are shown in Figure 13. This flash was a positive IC lightning flash and lasted for about 600 ms. Initially, the upper negative leader extended vertically upward, splitting into two channels at a height of 10.2 km and continued to develop upward in an inclined manner. About 190 ms after the lightning initiation, no location results were detected in the upper negative leader region. From 0 ms, corresponding to the moment of IEC waveform manifestation, until 190 ms, the fast antenna waveform continued to change without returning to zero.

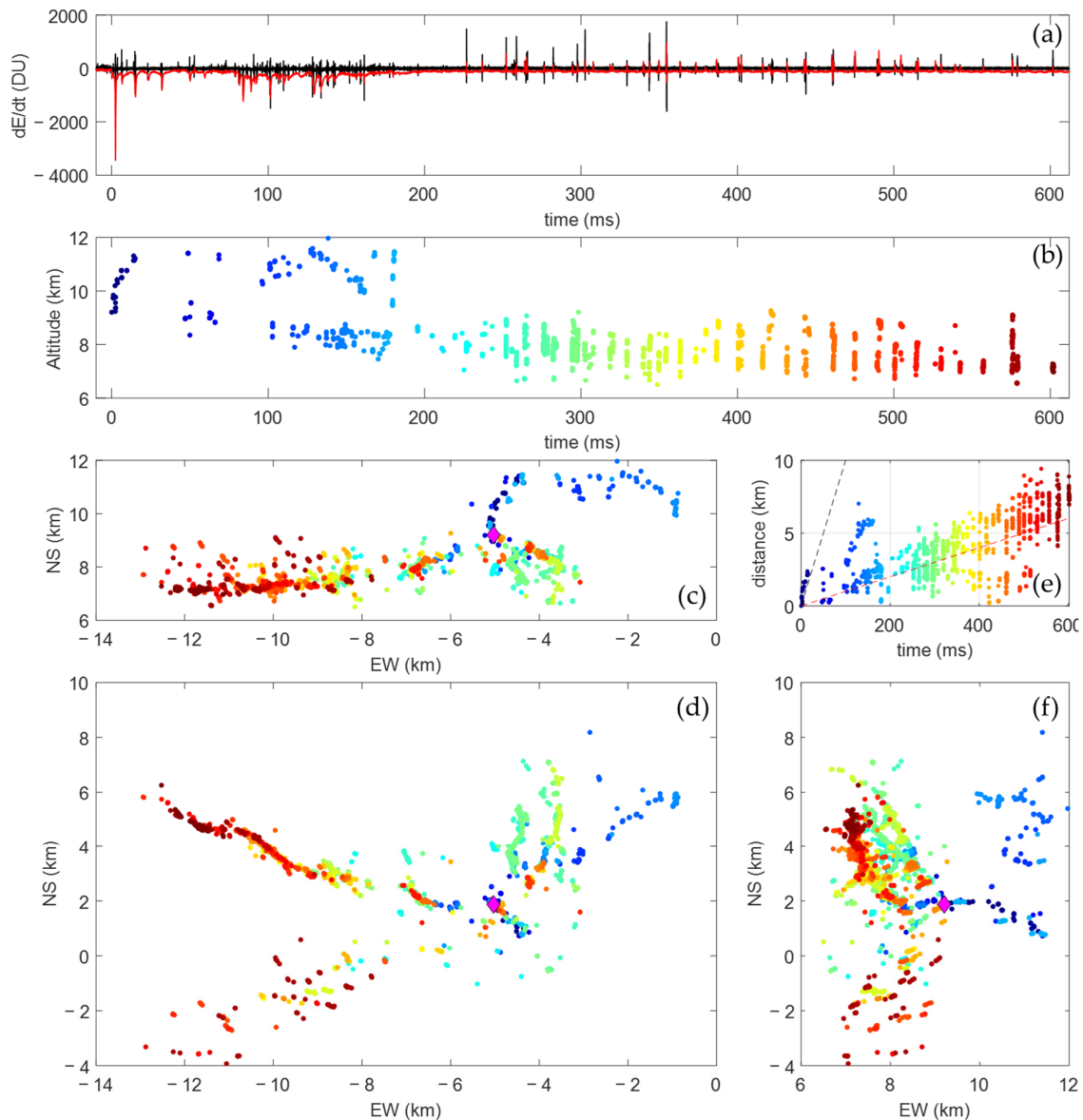


Figure 13. The entire location result of the IC lightning initiated by an initial breakdown pulse. (a) dE/dt (black) and fast antenna (red) waveforms. (b) The location result in the height–time view, with color changing from blue to red according to time. (c) Height–distance (from west to east) view. (d) Plan view. (e) Change in distance of radiation sources from initiation point over time. The red dashed line indicates a reference speed of 10^4 m/s, and the black dashed line represents a speed of 10^5 m/s. (f) Distance (from south to north)–height view. The magenta diamond stands for the initial point.

The development of the lower positive leader was observed at about 47 ms after the lightning initiation. Multiple instances of negative recoil leaders were also observed developing along the pre-existing positive channel toward the lightning initiation area. The positive leader, after developing downward from the initiation area within the 6.5–9.2 km altitude range. The positive channels originated from the lightning initiation area and developed into multiple branches, with a slanted downward development. Between the positive and negative channel branch points, there was a relatively vertical discharge channel, about 1 km in length, and the lightning initiation area was closer to the lower negative charge region.

Figure 14 shows the initial stage of this IC lightning, including waveforms detected by both the dE/dt sensor and fast antenna, and the location result of the lightning radi-

tion sources. The lightning initiation area was located ~ 4 km horizontally from the fast antenna detection sensor. The IEC on the fast antenna waveform exhibited a sustained negative shift and did not return to zero. Weak pulses were observed in the synchronized dE/dt waveform.

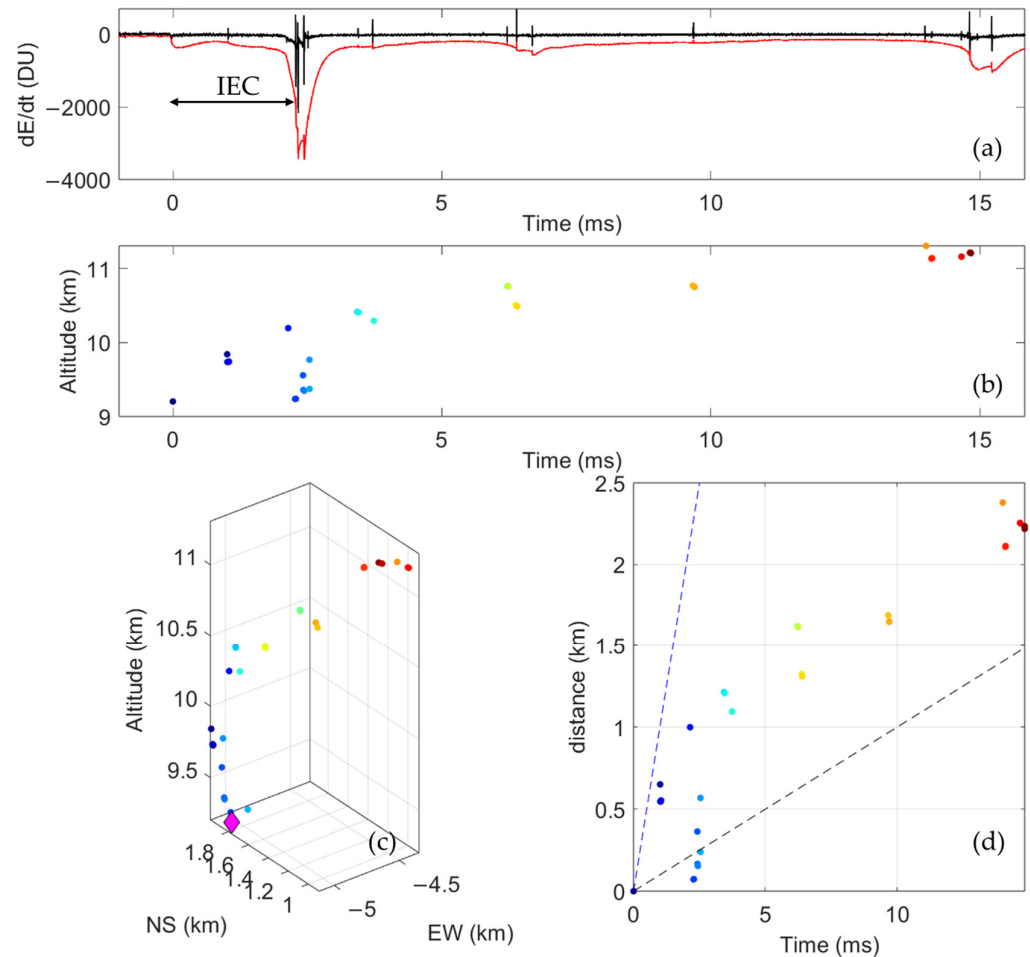


Figure 14. The location result of the lightning initiation by IEC during the initial 15 ms. (a) dE/dt (black) and fast antenna (red) waveforms. (b) Location result in height–time view, with color changing from blue to red according to time. (c) 3D view. The magenta diamond stands for the initial point. (d) Change in distance of radiation sources from initiation point over time. The blue dashed line indicates a reference speed of 10^6 m/s, and the black dashed line represents a speed of 10^5 m/s.

At the moment when the IEC began to enhance in the fast antenna waveform, the dE/dt antenna also detected subtle pulses. The sources associated with pulses in the dE/dt waveform were located at an altitude of 9.2 km and were considered to occur at the onset of the lightning. At about 1.1 ms, weak pulses were detected in both dE/dt and fast antenna waveforms, located at a height of 10 km.

Calculated from the initial positions, the propagation speed of the radiation sources was 6×10^5 m/s. About 2.1 ms after the lightning initiation, the first classic IBP was identified, with the localized radiation source at a height of 9.3 km. Both the dE/dt and fast electric field waveforms exhibited a positive change during the first half-cycle of the pulse, in contrast to the direction of the IEC waveform.

6. Discussion

A notable finding from the study was the detection of a flash initiated by the IEC. Both the dE/dt and the IEC were characterized by a slow negative waveform on the fast electric field change waveform, and no obvious pulses on both the dE/dt and the fast electric field

change waveforms, while the subsequent IBPs were characterized by bipolar pulses on both the dE/dt and fast electric field change waveforms.

As delineated by Formula (3) according to Uman [23], the lightning vertical electric field detected on the ground is constituted by three components, listed in sequence as: the electrostatic field, the induction field, and the radiation field.

$$E_z(D, t) = \frac{1}{2\pi\epsilon_0} \left(\begin{aligned} & \int_0^H \frac{(2-3\sin^2\theta)}{R^3} \times \int_0^t i(z, \tau - R/c) d\tau dz \\ & + \int_0^H \frac{(2-3\sin^2\theta)}{cR^2} i(z, t - R/c) dz \\ & - \int_0^H \frac{\sin^2\theta}{c^2R} \frac{\partial i(z, t - R/c)}{\partial t} dz \end{aligned} \right) \quad (3)$$

It is worth noting that when the discharge current appears and increases, the polarity of the radiation field component is opposite to that of the induction and electrostatic electric field components.

Considering the proximity of the IEC and subsequent IBPs in time and space, the decay of three electric field components with distance was similar. The differences in waveform characteristics and polarity variations illustrated significant disparities in the associated currents between the IEC and IBP processes.

The continuous unipolar field changes and absence of significant electric field pulses during the IEC indicates that the IEC emits larger electrostatic and induction field components with a smaller radiant field component. It can be inferred that there is a continuous discharge process with no significant current pulse in the discharge channel.

The pulse polarity change of the IBP bipolar pulse indicates that there is a strong radiation field component, which is caused by an abrupt current change. Importantly, the polarity in the initial half cycle of IBP is opposite to the waveform polarity of the IEC, indicating that the current propagation direction of the two processes is the same. Therefore, it can be inferred that IBP may be generated by air breakdown, and the pulse width of IBP reflects its discharge duration of more than ten microseconds.

Remarkably, the electric field change waveform similar to the IEC process persisted for about 190 ms in this paper, suggesting the presence of ongoing continuous current processes during the IBP phases. The current heating of the IEC may have contributed to the air breakdown discharge to some extent. The continuous current and frequent breakdowns might occur as the lightning initiated and developed. There are relatively few observations of IEC in the previous research [16,17], and in our observations, and one possible reason is that the rapid decay of the electrostatic and induction field components as the distance between the discharge and the sensor increases makes it difficult to detect the IEC process. This prolonged discharge phenomenon needs to be further investigated with additional observation and simulation studies.

7. Conclusions

In this paper, we reported the upgraded 3D LF-LMS in North China. The mapping results of a rocket-triggered lightning flash and three IC lightning flashes were used to study the initiation process of the lightning discharge. A dE/dt sensor without a time constant has been newly designed to detect frequent discharge pulses during the development of lightning channels. This upgraded 3D LF-LMS utilizes a continuous recording at a 20 MS/s sampling rate for hours, capturing the radiation signals of lightning activities of the passing thunderstorm. The continuous detection ensures a complete observation of the whole lightning discharge process, particularly the weak radiations that may be contained during the initial stage of the lightning.

The mapping results of rocket-triggered lightning are consistent with the observed optical detection channels with a location error less than 100 m in both horizontal and vertical directions, which proved the system's ability to precisely locate and distinguish the 3D development of lightning discharge channels.

The continuous detection of the upgraded 3D LF-LMS ensured that the initial stage of lightning can be effectively located and mapped. Three IC flashes, mapped by the

upgraded lightning location network, initiated from three types, typical IBP, NBE, and IEC. Based on the development speed of the leader's head and the characteristics of the negative recoil leader, the area of the different polarity channel's extensions was clearly identified. All three IC flashes were positive and occurred in the dipole charge structure of the thundercloud with the upper positive and lower negative charge regions. After the initiation of the lightning, an upward negative leader was initially located, followed by scatter radiation sources and negative recoil leaders in the lower negative charge region. The continuous current and frequent breakdowns might occur on the lightning discharge channel following its initiation between positive and negative charge regions.

Author Contributions: Conceptualization, M.L. and X.Q.; methodology, M.L.; software, M.L.; validation, M.L.; formal analysis, M.L. and Z.S.; investigation, M.L., X.Q., Z.S., R.J., H.Z., R.C. and S.Y.; resources, M.L., Z.S., Y.W. and X.L.; data curation, M.L.; writing—original draft preparation, M.L.; writing—review and editing, M.L., Z.S. and X.Q.; visualization, M.L.; supervision, X.Q.; project administration, X.Q. and R.J. All authors have read and agreed to the published version of the manuscript.

Funding: This research was funded by the National Natural Science Foundation of China (Grants. 42027803, 42230609 and 42322505).

Data Availability Statement: The data presented in this study are available on request from the corresponding author.

Acknowledgments: Thanks to all members of the lightning group of the Institute of Atmospheric Physics, Chinese Academy of Sciences for their assistance in the experiment. We are also thankful to the reviewers for their helpful feedback.

Conflicts of Interest: Author Yu Wang was employed by the company NARI Group Corporation Ltd. The remaining authors declare that the research was conducted in the absence of any commercial or financial relationships that could be construed as a potential conflict of interest.

References

1. Rakov, V.A. Electromagnetic Methods of Lightning Detection. *Surv. Geophys.* **2013**, *34*, 731–753. [[CrossRef](#)]
2. Lyu, F.; Cummer, S.A.; Solanki, R.; Weinert, J.; McTague, L.; Katko, A.; Barrett, J.; Zgoneanu, L.; Xie, Y.; Wang, W. A Low-Frequency near-Field Interferometric-TOA 3-D Lightning Mapping Array. *Geophys. Res. Lett.* **2014**, *41*, 7777–7784. [[CrossRef](#)]
3. Wang, Y.; Qie, X.; Wang, D.; Liu, M.; Su, D.; Wang, Z.; Liu, D.; Wu, Z.; Sun, Z.; Tian, Y. Beijing Lightning Network (BLNET) and the Observation on Preliminary Breakdown Processes. *Atmos. Res.* **2016**, *171*, 121–132. [[CrossRef](#)]
4. Wu, T.; Wang, D.; Takagi, N. Lightning Mapping with an Array of Fast Antennas. *Geophys. Res. Lett.* **2018**, *45*, 3698–3705. [[CrossRef](#)]
5. Zhu, Y.; Bitzer, P.; Stewart, M.; Podgorny, S.; Corredor, D.; Burchfield, J.; Carey, L.; Medina, B.; Stock, M. Huntsville Alabama Marx Meter Array 2: Upgrade and Capability. *Earth Space Sci.* **2020**, *7*, e2020EA001111. [[CrossRef](#)]
6. Fan, X.P.; Zhang, Y.J.; Zheng, D.; Zhang, Y.; Lyu, W.T.; Liu, H.Y.; Xu, L.T. A New Method of Three-Dimensional Location for Low-Frequency Electric Field Detection Array. *J. Geophys. Res. Atmos.* **2018**, *123*, 8792–8812. [[CrossRef](#)]
7. Stock, M.; Wu, T.; Akiyama, Y.; Ushio, T.; Kawasaki, Z.; Nakamura, Y.; Stock, M.; Kawasaki, Z. Improvements to the BOLT Lightning Location System. In Proceedings of the 2016 33rd International Conference on Lightning Protection (ICLP), Estoril, Portugal, 25–30 September 2016; IEEE: Estoril, Portugal, 2016; pp. 1–4. [[CrossRef](#)]
8. Ma, Z.; Jiang, R.; Qie, X.; Xing, H.; Liu, M.; Sun, Z.; Qin, Z.; Zhang, H.; Li, X. A Low Frequency 3D Lightning Mapping Network in North China. *Atmos. Res.* **2021**, *249*, 105314. [[CrossRef](#)]
9. Yuan, S.; Qie, X.; Jiang, R.; Wang, D.; Sun, Z.; Srivastava, A.; Williams, E. Origin of an Uncommon Multiple-Stroke Positive Cloud-to-Ground Lightning Flash with Different Terminations. *JGR Atmos.* **2020**, *125*, e2019JD032098. [[CrossRef](#)]
10. Wang, Y.; Min, Y.; Liu, Y.; Zhao, G. A New Approach of 3D Lightning Location Based on Pearson Correlation Combined with Empirical Mode Decomposition. *Remote Sens.* **2021**, *13*, 3883. [[CrossRef](#)]
11. Karunarathne, S.; Marshall, T.C.; Stolzenburg, M.; Karunarathna, N.; Vickers, L.E.; Warner, T.A.; Orville, R.E. Locating Initial Breakdown Pulses Using Electric Field Change Network. *J. Geophys. Res. Atmos.* **2013**, *118*, 7129–7141. [[CrossRef](#)]
12. Yuan, S.; Jiang, R.; Qie, X.; Wang, D. Side Discharges from the Active Negative Leaders in a Positive Cloud-To-Ground Lightning Flash. *Geophys. Res. Lett.* **2021**, *48*, e2021GL094127. [[CrossRef](#)]
13. Clarence, N.D.; Malan, D.J. Preliminary Discharge Processes in Lightning Flashes to Ground. *Q. J. R. Meteorol. Soc.* **1957**, *83*, 161–172. Available online: <https://rmets.onlinelibrary.wiley.com/doi/10.1002/qj.49708335603> (accessed on 9 April 2024). [[CrossRef](#)]

14. Nag, A.; DeCarlo, B.A.; Rakov, V.A. Analysis of Microsecond- and Submicrosecond-Scale Electric Field Pulses Produced by Cloud and Ground Lightning Discharges. *Atmos. Res.* **2009**, *91*, 316–325. [[CrossRef](#)]
15. Nag, A.; Rakov, V.A. Some Inferences on the Role of Lower Positive Charge Region in Facilitating Different Types of Lightning. *Geophys. Res. Lett.* **2009**, *36*, L05815. [[CrossRef](#)]
16. Marshall, T.; Stolzenburg, M.; Karunarathna, N.; Karunarathne, S. Electromagnetic Activity before Initial Breakdown Pulses of Lightning. *J. Geophys. Res. Atmos.* **2014**, *119*, 12558–12574. [[CrossRef](#)]
17. Marshall, T.; Bandara, S.; Karunarathne, N.; Karunarathne, S.; Kolmasova, I.; Siedlecki, R.; Stolzenburg, M. A Study of Lightning Flash Initiation Prior to the First Initial Breakdown Pulse. *Atmos. Res.* **2019**, *217*, 10–23. [[CrossRef](#)]
18. Rison, W.; Krehbiel, P.R.; Stock, M.G.; Edens, H.E.; Shao, X.-M.; Thomas, R.J.; Stanley, M.A.; Zhang, Y. Observations of Narrow Bipolar Events Reveal How Lightning Is Initiated in Thunderstorms. *Nat. Commun.* **2016**, *7*, 10721. [[CrossRef](#)]
19. Tilles, J.N.; Liu, N.; Stanley, M.A.; Krehbiel, P.R.; Rison, W.; Stock, M.G.; Dwyer, J.R.; Brown, R.; Wilson, J. Fast Negative Breakdown in Thunderstorms. *Nat. Commun.* **2019**, *10*, 1648. [[CrossRef](#)] [[PubMed](#)]
20. Qie, X.; Jiang, R.; Yang, J. Characteristics of Current Pulses in Rocket-Triggered Lightning. *Atmos. Res.* **2014**, *135–136*, 322–329. [[CrossRef](#)]
21. Qie, X.; Zhao, Y.; Zhang, Q.; Yang, J.; Feng, G.; Kong, X.; Zhou, Y.; Zhang, T.; Zhang, G.; Zhang, T.; et al. Characteristics of Triggered Lightning during Shandong Artificial Triggering Lightning Experiment (SHATLE). *Atmos. Res.* **2009**, *91*, 310–315. [[CrossRef](#)]
22. Chan, Y.T.; Ho, K.C. A Simple and Efficient Estimator for Hyperbolic Location. *IEEE Trans. Signal Process.* **1994**, *42*, 1905–1915. [[CrossRef](#)]
23. Uman, M.A.; McLain, D.K.; Krider, E.P. The Electromagnetic Radiation from a Finite Antenna. *Am. J. Phys.* **1975**, *43*, 33–38. [[CrossRef](#)]
24. Yoshida, S.; Wu, T.; Ushio, T.; Kusunoki, K.; Nakamura, Y. Initial Results of LF Sensor Network for Lightning Observation and Characteristics of Lightning Emission in LF Band. *J. Geophys. Res. Atmos.* **2014**, *119*, 12034–12051. [[CrossRef](#)]
25. Zhang, H.; Zhang, Y.; Fan, Y.; Zhang, Y.; Krehbiel, P.R.; Lyu, W. Guangdong Lightning Mapping Array: Errors Evaluation and Preliminary Results. *Earth Space Sci.* **2023**, *10*, e2023EA003143. [[CrossRef](#)]
26. Sun, Z.; Qie, X.; Liu, M.; Cao, D.; Wang, D. Lightning VHF Radiation Location System Based on Short-Baseline TDOA Technique—Validation in Rocket-Triggered Lightning. *Atmos. Res.* **2013**, *129–130*, 58–66. [[CrossRef](#)]

Disclaimer/Publisher’s Note: The statements, opinions and data contained in all publications are solely those of the individual author(s) and contributor(s) and not of MDPI and/or the editor(s). MDPI and/or the editor(s) disclaim responsibility for any injury to people or property resulting from any ideas, methods, instructions or products referred to in the content.